Nuclear Engineering and Design 244 (2012) 61–72

Contents lists available at SciVerse ScienceDirect

Nuclear Engineering and Design

journal homepage: www.elsevier.com/locate/nucengdes

A numerical and three-dimensional analysis of steady state rectangular natural circulation loop

G. Angelo [a,b,*], D.A. Andrade [a], E. Angelo [a,b], W.M. Torres [a], G. Sabundjian [a], L.A. Macedo [a], A.F. Silva [b]

[a] Instituto de Pesquisas Energéticas e Nucleares, Avenida Lineu Prestes, 2242, Centro de Engenharia Nuclear, CEP 05508-000, São Paulo, SP, Brazil
[b] Universidade Presbiteriana Mackenzie, Rua da Consolação, 930, CEP 01302-907, São Paulo, SP, Brazil

ARTICLE INFO

Article history:
Received 21 June 2011
Received in revised form 7 December 2011
Accepted 13 December 2011

ABSTRACT

Free convection circuits or natural circulation systems are employed in several engineering fields. In nuclear reactors, natural circulation can be used as a passive safety system or as a main heat transfer mechanism.

This work presents the results of a three-dimensional numerical analysis of a steady state rectangular natural circulation loop located at the Instituto de Pesquisas Energéticas e Nucleares/Comissão Nacional de Energia Nuclear (IPEN/CNEN-SP). Numerical results and experimental data present in this paper are discussed and compared.

The model is good enough to capture 3-D effects, such as the formation of vortex structures and swirl effects.

1. Introduction

The free convection phenomenon occurs without any mechanical devices intervention when the field forces acting on the fluid present density gradients able to induce free convection.

Free convection circuits or natural circulation systems are employed in several engineering fields such as: (i) water heating by solar energy (thermo-siphons shown schematically in Fig. 1a); (ii) thermal control of electronic components (Teertstra et al., 2006); (iii) geothermal energy (shown schematically in Fig. 1b); (iv) nuclear reactors where natural circulation can be used as a passive safety system (IAEA-TECDOC, 2005) or main heat transfer device (Ingersoll, 2009) (Fig. 1c shows a cross section of a Lead-Cooled Fast Reactor).

Specifically in nuclear reactors, natural circulation is used as a passive safety system (IAEA-TECDOC, 2005; Carelli et al., 2004) which means that, in critical situations, without any external device, the system provides the stable safety for its own operating characteristics. The natural convection system is independent of human actions and results from the lessons of historical accidents that occurred due to a succession of human mistakes under critical operation conditions, such as Three Mile Island and Chernobyl.

Some nuclear reactors, such as Multi-Application Small Light Water Reactor (MASLWR) (IAEA-TECDOC, 2005) and Lead-Cooled Fast Reactor (LCFR) (Ingersoll, 2009), intend to work only under natural circulation phenomena.

Zvirin (1982) and Greif (1988) wrote two of the most important paper reviews on this subject. Their works present experimental and theoretical natural circulation loops for a single-phase flow regime. These articles discuss analytical and numerical methods for different circuit designs such as: (i) simple geometries; (ii) small-scale systems; (iii) nuclear reactors and (iv) thermo-siphons.

Vijayan's work (Vijayan, 2002) states that single-phase steady state natural circulation loops with variable or constant flow cross sections can be expressed as a relationship between two non-dimensional groups. The correlation proposed was tested against experimental data from various loops and showed a reasonable agreement.

One-dimensional models widely reported in the literature (Zvirin, 1982; Greif, 1988; Huang and Zelaya, 1988; Jiang et al., 2002) consider velocity and temperature averages in the flow cross sections. In this approach, the friction factor, the loss coefficients and the heat transfer coefficients must be specified. The velocity is assumed only in the axial direction and the curvature effects and the axial conduction are disregarded. The momentum equation is reduced to an overall balance between friction and buoyancy.

In order to obtain more realistic results, a (1D/2D) one-dimensional/two-dimensional methodology was proposed by Mertol et al. (1982) followed by Bernier and Baliga (1992), Su

* Corresponding author at: Instituto de Pesquisas Energéticas e Nucleares, Avenida Lineu Prestes, 2242, Centro de Engenharia Nuclear, CEP 05508-000, São Paulo, SP, Brazil. Tel.: +55 1131339496; fax: +55 1131339496.
E-mail addresses: gabriel.angelo@usp.br, gabriel.angelos@gmail.com (G. Angelo), delvonei@ipen.br (D.A. Andrade), eangelo@mackenzie.br (E. Angelo), wmtorres@ipen.br (W.M. Torres), gdjian@ipen.br (G. Sabundjian), lamacedo@ipen.br (L.A. Macedo), nagu@terra.com.br (A.F. Silva).

0029-5493/$ – see front matter © 2012 Elsevier B.V. All rights reserved.
doi:10.1016/j.nucengdes.2011.12.020

Nomenclature

K	thermal conductivity (W/mK)
k	turbulent kinetic energy (m^2/s^2)
T	temperature (°C, K)
u_i	fluid velocity component (m/s)
$\overline{u_i u_j}$	Reynolds stress (m^2/s^2)
$\overline{u_i T}$	turbulent heat flux (mK/s)
α	thermal diffusivity (m^2/s)
β	thermal expansion coefficient (1/K)
ε	turbulent energy dissipation rate (m^2/s^3)
μ	dynamic viscosity (kg/ms)
ν	kinematic viscosity (m^2/s)

Superscripts

–	average value
′	fluctuation component

Subscripts

eff	effective
t	turbulent

$k-\varepsilon$

C_μ	0.09
σ_k	1.00
σ_ε	1.30
σ_θ	0.90
$C_{\varepsilon 1}$	1.44
$C_{\varepsilon 2}$	1.92

and Chen (1995), Misale et al. (1999) and, recently, by Basran and Kücüka (2003).

Desrayaud et al. (2006) numerically investigated an unsteady two-dimensional toroidal loop in several conditions and geometries. The model uses classical governing equation form (Navier–Stokes plus energy) for unsteady, incompressible and Newtonian fluid with the Buossinesq approximation. The two-dimensional approach was able to capture recirculation regions, periodic motion and Lorenz-like chaotic flow.

A long search into scientific databases, has led to only three articles dealing with three-dimensional numerical simulations under single-phase natural circulation phenomena. Lavine et al. (1987) was the precursor of the three-dimensional analysis in toroidal loops. Recently, Ambrosini et al. (2004) and Pilkhwal et al. (2007) presented a three-dimensional analysis of the hydrodynamic stability of rectangular loops in various positions of the heaters and coolers. They compared the results with those supplied by several types of software as well as with experimental results. In their studies, the RNG $k-\epsilon$ model was employed for turbulence treatment and, according to the authors, the coarse tetrahedral mesh in radial direction can be suppressed by the use of wall functions. Since the three-dimensional axial element size was based on one-dimensional node size, it is possible that the recirculation effects such as vortex formations could not be predicted with great accuracy.

Our three-dimensional steady state computational fluid dynamic model was developed for a natural circulation loop located at the Instituto de Pesquisas Energticas e Nucleares IPEN/CNEN-SP. The validation of the computational model is made by comparison with experimental data. The proposed model was able to capture tree-dimensional effects such as the formation of vortex structures and swirl effects and also pointed out that a one-dimensional/

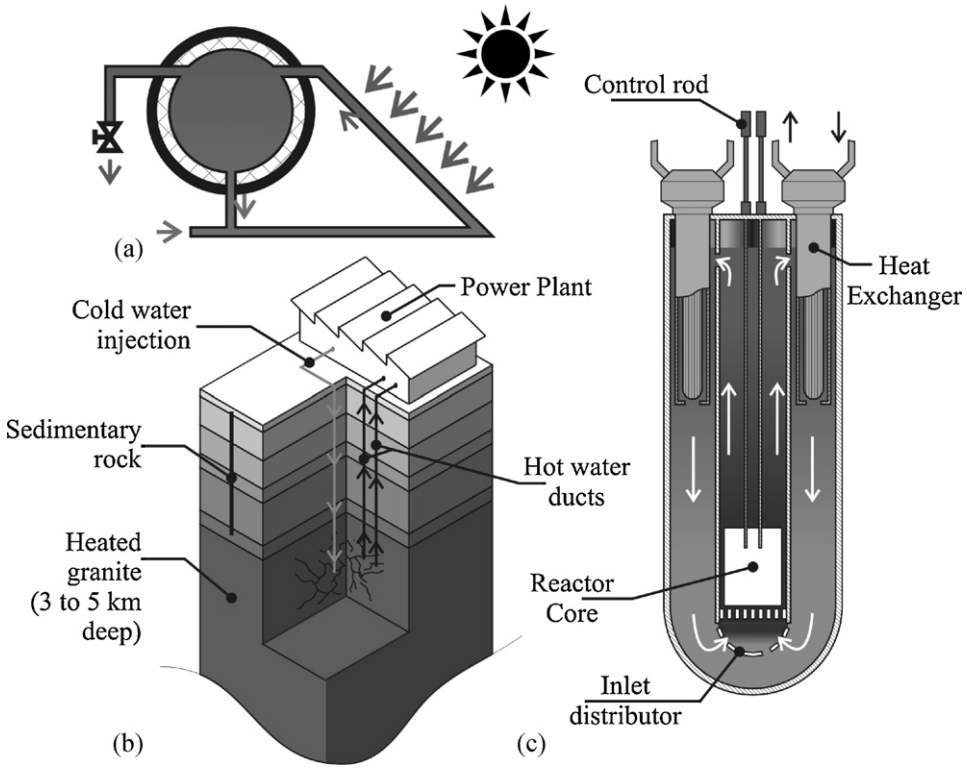

Fig. 1. (a) Schematic drawing of a thermo-siphon, (b) illustration of a geothermal Power station and (c) (modified by the author) cross section of a Lead-Cooled Fast Reactor (Ingersoll, 2009).

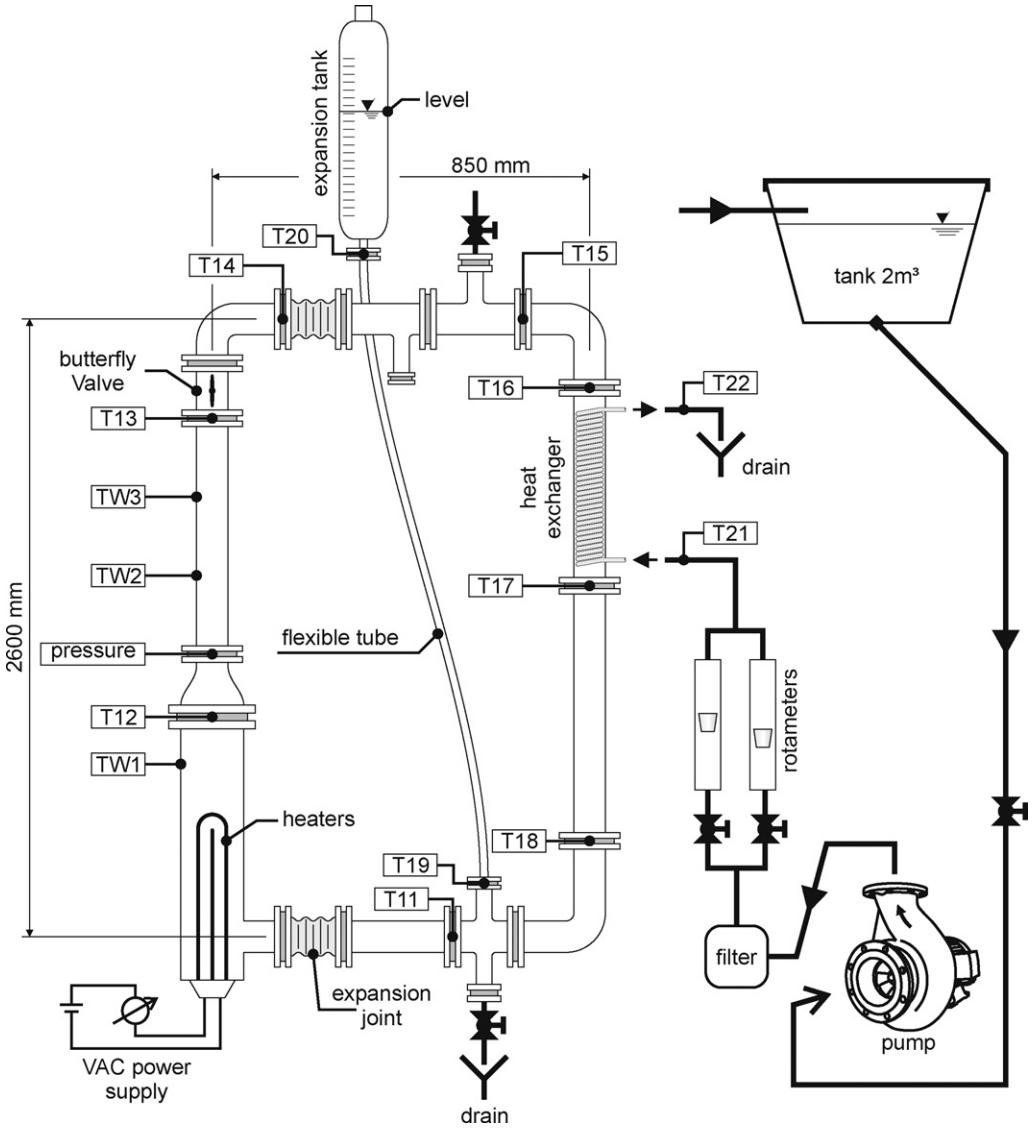

Fig. 2. Schematic natural circulation diagram.

tree-dimensional methodology can be used to reduce the computational effort.

2. Experimental data

The experimental circuit consists of a rectangular glass loop with an electric heater as the heat source and a coil cooler as the heat sink. Glass is used in the entire circuit to allow the flow visualization in order to identify the flow patterns. The main dimensions of the circuit as well as the thermocouple positions are indicated in Fig. 2.

Nine thermocouples were installed along the centerline of the loop to measure the temperature in the center of the tube. These thermocouples are installed in glass pipe joints using a polyester device; Fig. 3 shows the layout of the described device. Three thermocouples were installed outside the glass wall (Fig. 2 – TW1, TW2 and TW3). Measurements are recorded by a data acquisition system supplied by National Instruments Corporation. All the installed thermocouples are a K-type and have 1-millimeter diameter.

The data acquisition system is supplied by the National Instruments Corporation. It consists of two signal conditioner modules, two terminal blocks and an acquisition PCMCIA card installed into a notebook computer. Labview is used to create a visual software interface. Labview® is used to create a visual software interface.

The heating section has two electrical resistances and the applied power is controlled in the range from 0 to 8400 W (each electrical resistance ranges from 0 to 4200 W). The heat power is imposed through an alternate voltage controller. The main dimensions are shown in Fig. 4a.

The heat exchanger is a shell and tube device. If there is absence of reversal flow, this heat exchanger is a counter current type. It is composed of one shell and two concentric spirals (tube): the primary water circuit flows inside the shell while the refrigeration water flows inside the spirals. Fig. 4b schematically shows the main dimensions of the heat exchanger.

Experimental data are obtained as follows: (i) verification of the homogeneity of the thermocouple measures (initial temperatures); (ii) initialization of the secondary cooling system and adjustment of the mass flow rate through rotameters ($2.772 \times 10^{-2} \pm 1.38 \times 10^{-3}$ kg/s); (iii) adjustment of the nominal power.

The circuit is considered in steady state regime when the rate of change of the average temperature in time is approximately zero ($d\overline{T}/dt \cong 0$). Beyond this point and forward, the mean value and standard deviation are estimated. This calculation was performed

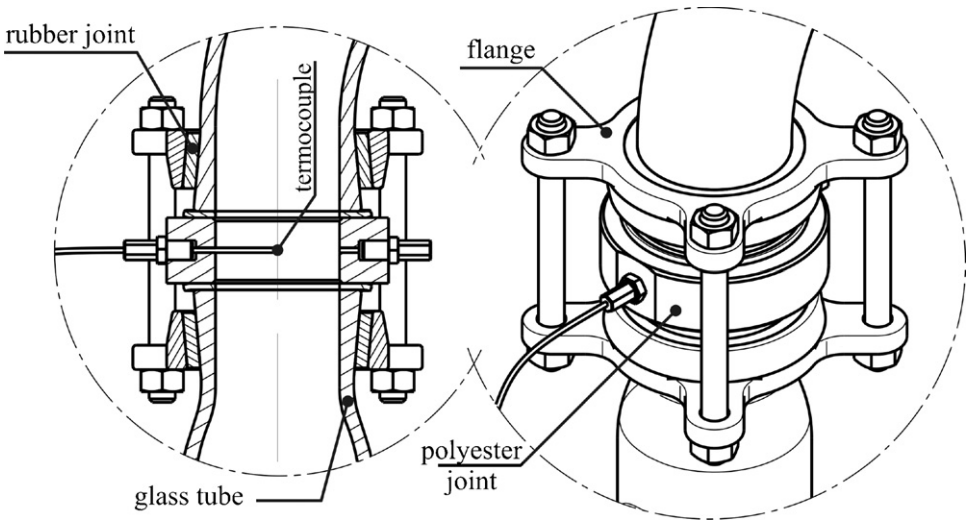

Fig. 3. Polyester device and thermocouple position.

for an interval of thirty measures in order to avoid corrections with Student's t (Bevington and Robinson, 1969).

Fig. 5 shows the average of the thirty experimental measurements as a function of time for thermocouple T12 and a nominal power of 1000 W. The total standard deviation (error bars) include the standard deviation associated with the usage of this type of thermocouple (±1 °C).

Table 1 presents the mean temperature and standard deviation for all the measures of the circuit in steady state regime. The values measured by thermocouples T19, T20, TW1, TW2 and TW3 are not shown, since the numerical model does not include such regions. Besides, T19 and T20 thermocouples present siphon geometry in flexible tube, which does not allow the heated fluid to reach the expansion tank. Finally, the experiments show that the water level in the expansion tank remains constant in single-phase flow regime.

3. Methodology

A tridimensional model for the natural circulation loop was developed based on the finite volume method applied to a tetrahedral unstructured mesh (Maliska, 1994; Anderson and Wendt, 1995). The mass, the momentum and energy conservation equations are considered. The turbulence model used is the standard $k-\varepsilon$ (Launder and Spalding, 1974). Ansys-CFX® code is used as the CFD tool.

The mathematical model considers the time averaging in the conservation equations for the following hypotheses: (i) incompressible fluid, (ii) Newtonian fluid and (iii) Buossinesq assumption for the Reynolds stresses $(-\rho\overline{u'_i u'_j} = \mu_t(\partial\overline{u}_i/\partial x_j + \partial\overline{u}_j/\partial x_i) - (2/3)\rho k)$ and the turbulent heat flux $(-\overline{u'_j T} = \alpha_t(\partial\overline{T}/\partial x_i))$. Thus the average conservation equations for the mass, the momentum and energy are given respectively by Eqs. (1), (2) and (3).

$$\frac{\partial\overline{u}_i}{\partial x_i} = \frac{\partial u'_i}{\partial x_i} = 0 \tag{1}$$

$$\rho\frac{\partial\overline{u}_i}{\partial t} + \rho\frac{\partial}{\partial x_i}\left(\overline{u}_i\,\overline{u}_j\right) = -\frac{\partial p^*}{\partial x_i} + \frac{\partial}{\partial x_j}\left(\mu_{eff}\left(\frac{\partial\overline{u}_i}{\partial x_j} + \frac{\partial\overline{u}_j}{\partial x_i}\right)\right) + S_M, \tag{2}$$

where p^* is the modified pressure ($p^* = p + (2/3)\rho k$), $k = (1/2)\overline{u'_i u'_i}$ and $\mu_{eff} = \mu + \mu_t$.

$$\frac{\partial\overline{T}}{\partial t} + \frac{\partial}{\partial x_i}\left(\overline{u}_i\,\overline{T}\right) = \frac{\partial}{\partial x_i}\left(\alpha_{eff}\frac{\partial\overline{T}}{\partial x_i}\right), \tag{3}$$

where $\alpha_{eff} = \alpha + \alpha_t$ and α_t is obtained by Eq. (4).

$$\alpha_t = \frac{\mu_t}{\rho Pr_t}, \tag{4}$$

where Pr_t is the turbulent Prandtl number.

Since the $k-\varepsilon$ model was used, the turbulent eddy viscosity is defined by Eq. (5). The transport equations for turbulent kinetic energy (k) and the turbulent dissipation rate (ε) are presented in Eqs. (6) and (7).

$$\mu_t = C_\mu\rho\frac{k^2}{\varepsilon} \tag{5}$$

$$\rho\frac{\partial k}{\partial t} + \rho\frac{\partial}{\partial x_i}(\overline{u}_i\,k) = \frac{\partial}{\partial x_i}\left(\left(\mu + \frac{\mu_t}{\sigma_k}\right)\frac{\partial k}{\partial x_i}\right) + P_k + P_{kb} - \rho\,\varepsilon \tag{6}$$

$$\rho\frac{\partial\varepsilon}{\partial t} + \rho\frac{\partial}{\partial x_i}(\overline{u}_i\,\varepsilon) = \frac{\partial}{\partial x_i}\left(\left(\mu + \frac{\mu_t}{\sigma_\varepsilon}\right)\frac{\partial\varepsilon}{\partial x_i}\right) + \frac{\varepsilon}{k}(C_{\varepsilon 1}(P_k + P_{\varepsilon b}) - C_{\varepsilon 2}\rho\,\varepsilon) \tag{7}$$

where P_k is the shear production of turbulence (Eq. (8)), P_{kb} is the buoyancy turbulence production (Eq. (9)) and $P_{\varepsilon b}$ is the buoyancy turbulence dissipation (Eq. (10)).

$$P_k = \mu_t\left(\frac{\partial\overline{U}_i}{\partial x_j} + \frac{\partial\overline{U}_j}{\partial x_i}\right)\frac{\partial\overline{U}_i}{\partial x_j} \tag{8}$$

$$P_{kb} = -g_i\beta\frac{\mu_t}{\sigma_\theta}\frac{\partial\overline{T}}{\partial x_i} \tag{9}$$

$$P_{\varepsilon b} = g_i\frac{\mu_t}{\sigma_\theta}\frac{\partial\overline{T}}{\partial x_i} \tag{10}$$

The buoyancy effect is modeled by the inclusion of a source term in the momentum equation as shown in Eq. (11).

$$S_{M,buoy} = (\rho - \rho_{ref})\cdot g_i, \tag{11}$$

where ρ is the fluid density and ρ_{ref} is the fluid reference density.

Since the pressure gradient is relatively small in the natural circulation loop and density variations are due to only temperature variations (Incropera and De Witt, 1985), the Boussinesq approximation was used as shown in Eq. (12).

$$S_{M,buoy} = -\rho_{ref}\cdot\beta\cdot g_i\cdot(T - T_{ref}), \tag{12}$$

where β is the thermal expansivity $\left(\beta = -(1/\rho)\cdot\partial\rho/\partial T\big|_p\right)$.

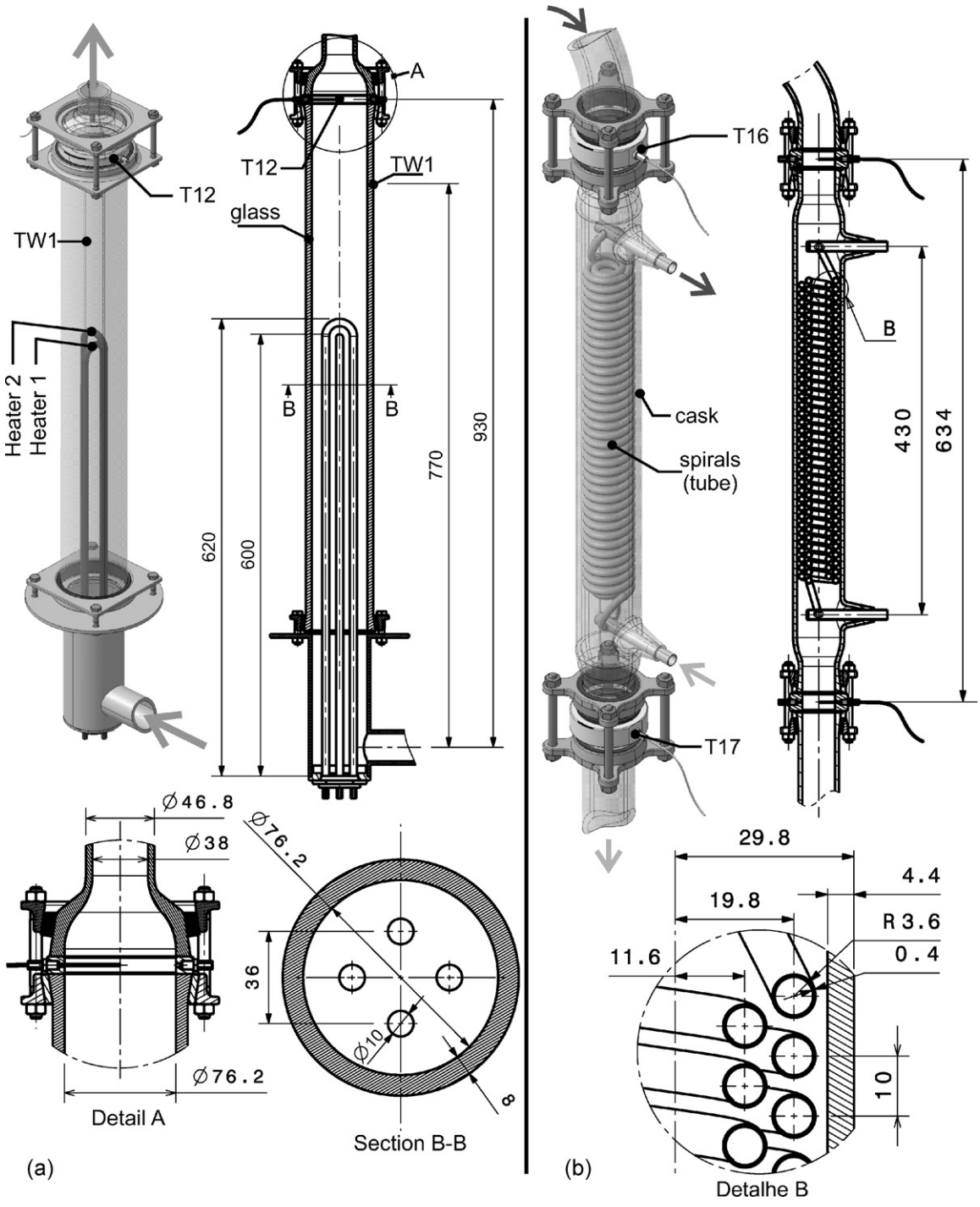

Fig. 4. (a) Detail view of the heated section, (b) detail view of the heat exchanger, all dimensions in millimeters.

The reference temperature is considered equal to room temperature ($T_{ref} = T_{env} = 25\,^{\circ}C$). The reference density is obtained as a function of the reference temperature $\rho_{ref} = \rho(T_{ref})$.

The fluid transport properties are taken exclusively as function of the average circuit temperature ($\mu = f(T_m)$, $k = f(T_m)$, $\beta = f(T_m)$) at constant pressure 101,325 Pa (atmospheric pressure) plus hydrostatic contribution due to the expansion tank. The average circuit temperature for each iteration is obtained by Eq. (13).

$$T_m = \frac{1}{\forall} \int_{\forall} T \, d\forall, \tag{13}$$

where $\forall$ is the computational domain volume.

The industrial IAPWS (International Association for the Properties of Water and Steam) formulations were used to acquire the new value of the water properties. Fig. 6 shows the water properties as a function of the reference temperature at constant pressure.

Heat losses to the environment are neglected.

Since there is no significant cross section variation in the expansion joints, the pressure drop in this regions is negligible.

The explicit geometry of the butterfly valve was not considered. However, the pressure drop ($-\partial P/\partial z$) in these device was simulated by a porous media with a constant resistance loss coefficient ($k_{eq} = 1.12$).

Table 1
Experimental measurements.

Nominal power	1000 W	1500 W	2000 W	2500 W
T11 (°C)	40.00 ± 0.507	45.48 ± 0.515	50.87 ± 0.505	55.73 ± 0.518
T12 (°C)	45.79 ± 0.511	52.32 ± 0.528	59.38 ± 0.508	65.12 ± 0.524
T13 (°C)	45.35 ± 0.505	51.89 ± 0.527	58.93 ± 0.503	64.66 ± 0.519
T14 (°C)	45.22 ± 0.506	51.75 ± 0.525	58.76 ± 0.504	64.47 ± 0.521
T15 (°C)	44.94 ± 0.507	51.52 ± 0.523	58.56 ± 0.504	64.31 ± 0.518
T16 (°C)	44.79 ± 0.504	51.31 ± 0.525	58.31 ± 0.505	63.96 ± 0.520
T17 (°C)	38.24 ± 0.522	43.32 ± 0.522	48.91 ± 0.509	53.77 ± 0.528
T18 (°C)	38.44 ± 0.506	43.49 ± 0.516	49.10 ± 0.505	53.98 ± 0.511
T21 (°C)	26.65 ± 0.503	26.92 ± 0.503	27.11 ± 0.504	27.67 ± 0.505
T22 (°C)	35.34 ± 0.546	39.48 ± 0.542	44.01 ± 0.532	48.08 ± 0.541
T_{env} (°C)	23.11 ± 0.623	25.91 ± 0.627	25.63 ± 0.660	26.21 ± 0.509
Power (W)	1023 ± 4.6	1484 ± 18.5	2029 ± 21.2	2530 ± 20.6

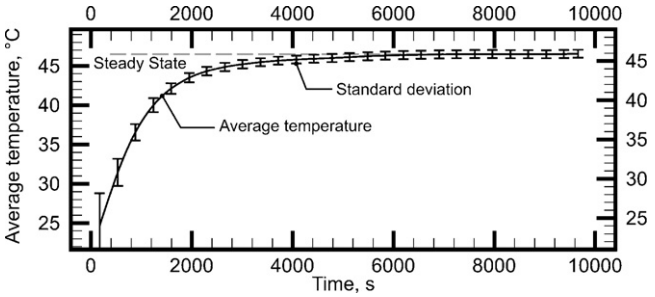

Fig. 5. Average temperature and standard deviation in a function of time for thermocouple T12, nominal power equal to 1000 W.

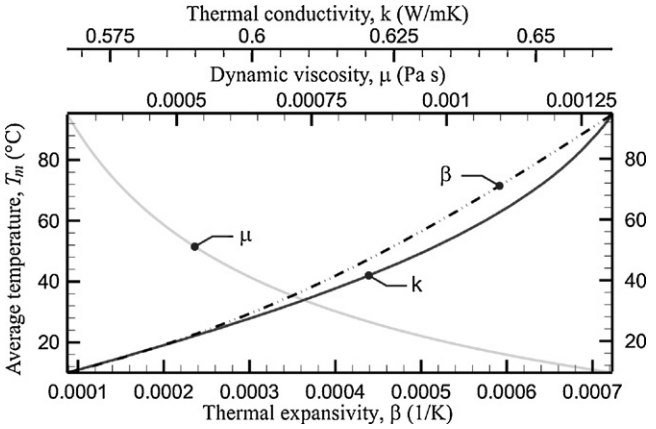

Fig. 6. Correction of water properties as a function of average circuit temperature (T_m).

In this article, the domain is symmetric and some geometric simplifications were considered in the heat exchanger as shown in Fig. 7. The original geometry has two concentric spirals (Fig. 7a). The numerical model considers it as a toroidal geometry (figure Fig. 7b) maintaining, however, the same heat transfer area and positions.

3.1. Boundary conditions

Heat flux ($\ddot{q}_{heater}$), non-slip and smooth walls are imposed on the surface of the electrical resistance as boundary conditions. The heat flux at the heater ranges from $25,250 \leqslant \ddot{q}_{heater} \leqslant 63,125\,W/m^2$ which is equivalent to $1000 \leqslant Q_{heater} \leqslant 2500$ W since the heat transfer area is constant. Since the power at the heater is less than 4200 W, only heater 1 is active. Fig. 8 shows the boundary condition for the entire model.

In steady state simulations, the boundary conditions such as heat flux in the heater surface and heat transfer coefficient (h, T_∞) in the heater exchanger region provide instabilities during the convergence process. Thus, a linear temperature distribution as a function of the length (Eq. (14)) and a non-slip and smooth wall were set as

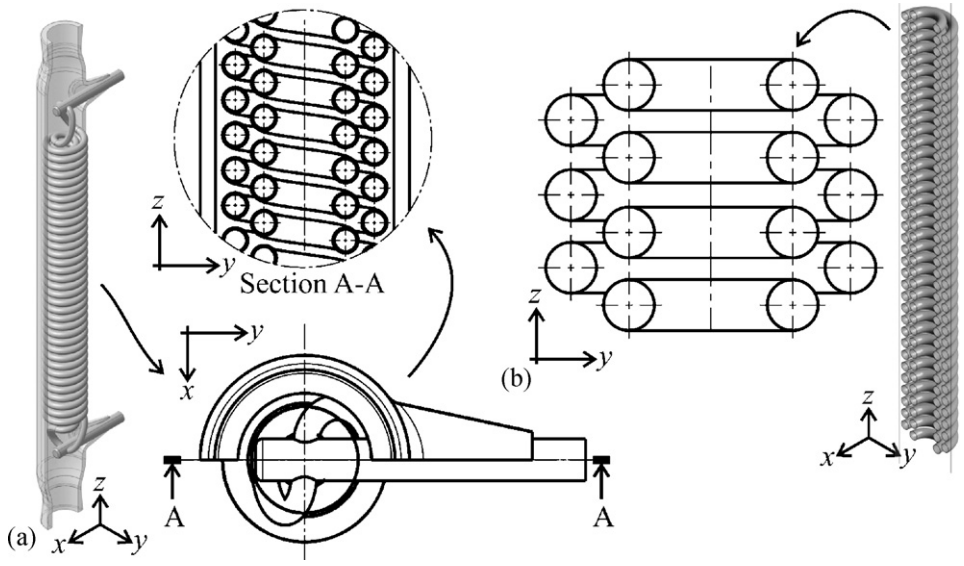

Fig. 7. Detail view of the heat exchanger (a) real heat exchanger geometry and (b) geometric simplification.

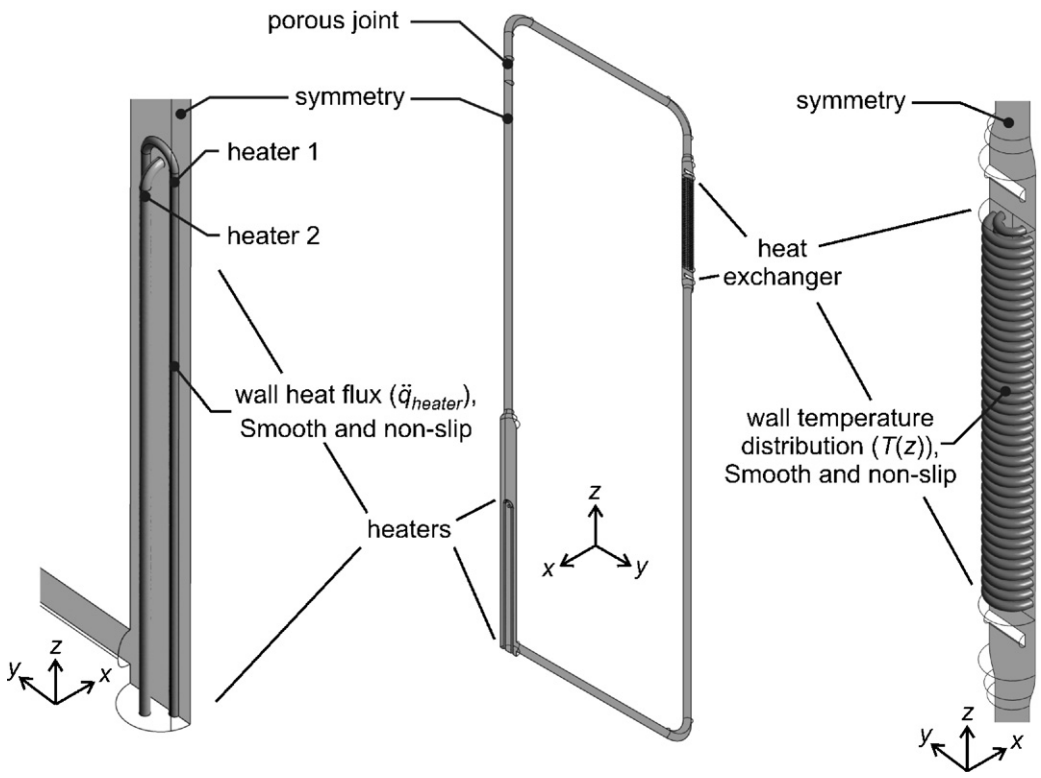

Fig. 8. Boundary conditions.

boundary conditions for the heat exchanger. Fig. 9 schematically shows the temperature distribution.

$$T_{HE}(z) = \frac{Q_{heater} \cdot z}{\dot{m}_{HE} \cdot cp \cdot L} + T_{in(HE)} \quad (14)$$

where $T_{in(HE)}$ is the heat exchanger secondary circuit inlet average temperature (T21), L is the heat exchanger total length, cp is the heat capacity at constant pressure, $\dot{m}_{HE}$ is the heat exchanger secondary circuit mass flow rate and z is a coordinate ranging from 0 to L.

The entire model was considered symmetric and all the other surfaces are non-slip, smooth and adiabatic walls. A summary of the boundary conditions for each case is presented in Table 2.

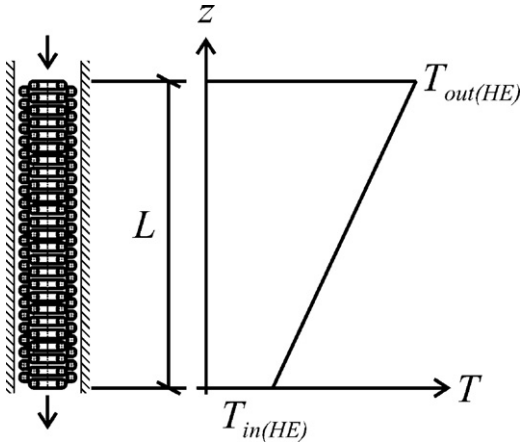

Fig. 9. Heat exchanger boundary condition.

3.2. Mesh

The approach presented by Stern et al. (2001) and Wilson et al. (2001) to define and verify the mesh is used in this paper. They discuss the mesh dependency on the results focusing the element size definition in order to validate the CFD models. The methodology considers an increase of the mesh density for the same boundary condition using predefined ratios. This procedure must be performed in such a way that property variation or small variations do not occur. When this condition is satisfied, the solution is considered independent of the mesh.

Fig. 10 shows the relationship for the number of elements and two independent variables: the temperature difference between point 1 and point 2 ($\Delta T_p = (T_{p1} - T_{p2})$) and the mass flow rate of the circuit ($\dot{m}$) for the same boundary conditions. The temperature variation for points (i) and (ii) is approximately 0.7% and 0.4% mass flow rate. Thus the calculations are performed for the mesh with 1.17 million elements.

Fig. 11 shows the mesh and two detailed views in the symmetry region. The General Grid Interface (GGI) (ANSYS, 2009) technique was used to connect the tetrahedrons and hexahedrons on the contact surfaces. This technique consists of the creation of a control surface treatment of the numerical fluxes across the interface. The numerical procedure is implicit and conservative in terms of mass, momentum and energy.

4. Results

Although experimental measurements are two-dimensional and numerical analyses are three-dimensional, a comparison with experimental data is made at the same geometric points, since a three-dimensional behavior is observed in the experiments, but not measured. Hence, it is assumed that the loop flow characteristic and behavior can be described with the numerical results.

Table 2
Boundary conditions.

Simulation	1	2	3	4
q''_{heater} (W)	21,250	31,875	42,500	53,125
$T_{in(HE)}$[a] (°C)	26.65	26.92	27.11	27.67
$T_{out(HE)}$[b] (°C)	35.4	39.8	44.4	49.2

[a] Experimental data.
[b] Obtained by Eq. (4).

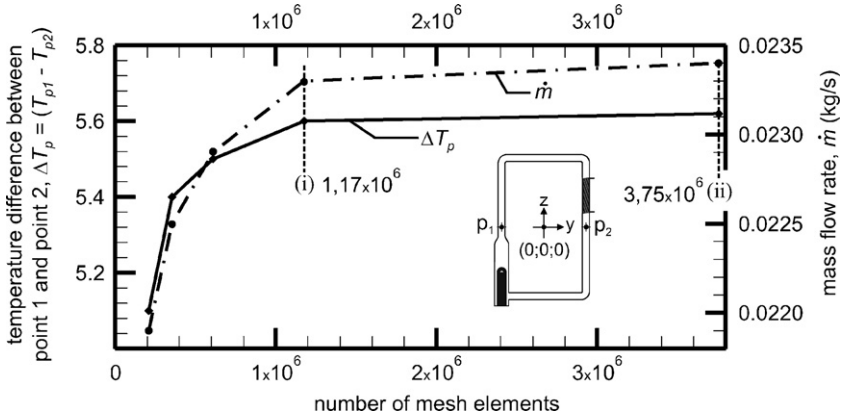

Fig. 10. Mesh sensitivity in results.

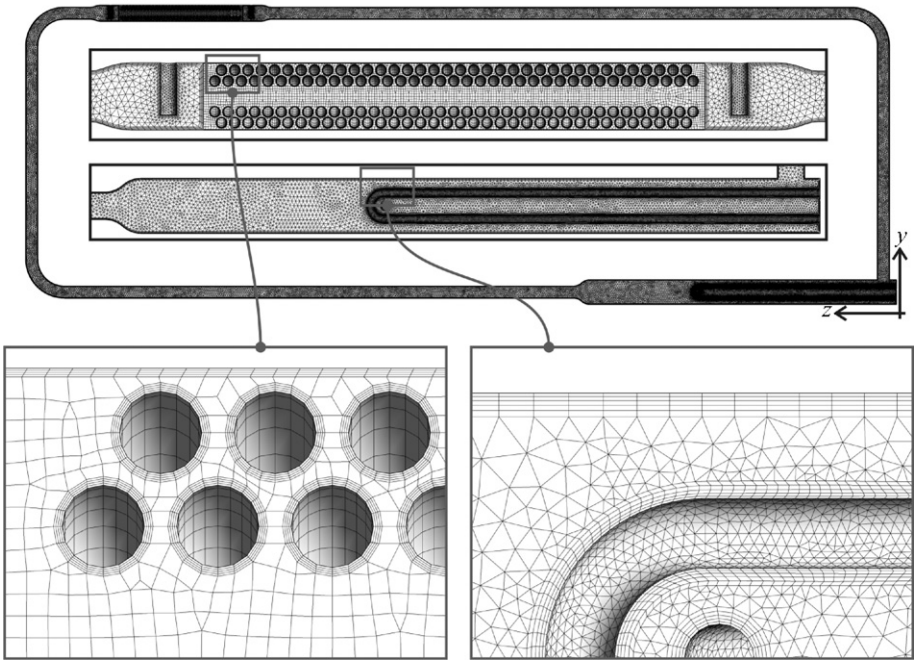

Fig. 11. Surface mesh of the symmetry region and detail view of the heater and heat exchanger.

Table 3
Numerical error.

	1000 W		1500 W		2000 W		2500 W	
	Num.	E(%)	Num.	E(%)	Num.	E(%)	Num.	E(%)
T11	37.09	4.00	42.67	2.27	46.60	5.47	48.44	10.61
T12	45.38	0.89	54.39	3.95	58.72	1.11	62.16	4.54
T13	45.34	0.02	54.42	4.87	58.71	0.38	62.14	3.90
T14	45.34	0.27	54.42	5.16	58.71	0.09	62.14	3.62
T15	45.36	0.93	54.43	5.65	58.72	0.27	62.15	3.36
T16	45.37	1.29	54.45	6.12	58.73	0.72	62.17	2.80
T17	37.66	1.51	43.49	0.39	47.58	2.71	49.54	7.87
T18	37.06	3.59	42.64	1.95	46.58	5.13	48.42	10.31

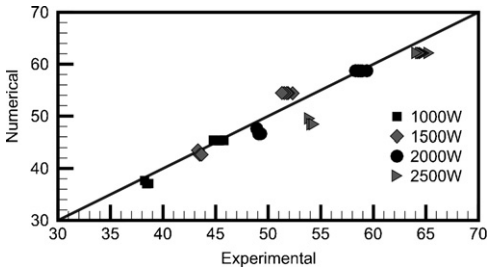

Fig. 12. Experimental data versus numerical results.

Fig. 12 shows a comparison between the numerical and experimental results. Table 3 shows the numerical results and the percentage deviation from the average experimental measurements (column indicated as $E(\%)$). The numerical model was found to systematically underestimate the circuit temperatures after the heat exchanger (T11, T17 and T18).

The underestimation can be related to: (i) the simplified geometry (toroid rather than helicoid), and (ii) the boundary conditions imposed as a linear distribution of temperatures and the heat exchanger wall temperature was set equal to the secondary circuit fluid temperature. These two simplifications promote a higher heat transfer rate resulting in lower temperatures at the outlet of the heat exchanger.

In the region after the heater, the temperatures obtained from the numerical model agree with the experimental measurements.

The ratio between the total height of the circuit and the distance on the z-axis is defined as $\zeta = z/H$ and H is equal to 2.6 metros (see Fig. 2).

Fig. 13 shows the velocity profiles in the heater region ($-0.015 \leqslant \zeta \leqslant 0.223$) for an applied power of 1000 W in heater 1. Near the inlet heated section ($\zeta = 0.03$), due to vortex structures and swirl effects in the device (Fig. 14a), a reversal flow located at $0.86 \leqslant \psi \leqslant 1.0$ is verified.

The swirl and vortex structures are also observed at post heated zone as observed in Fig. 14b.

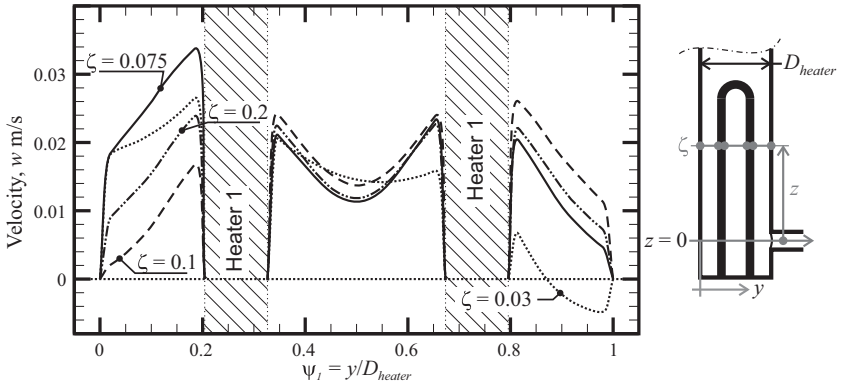

Fig. 13. Velocity profiles for heated zone $-0.015 \leqslant \zeta \leqslant 0.223$, Q_{heater} =1000 W.

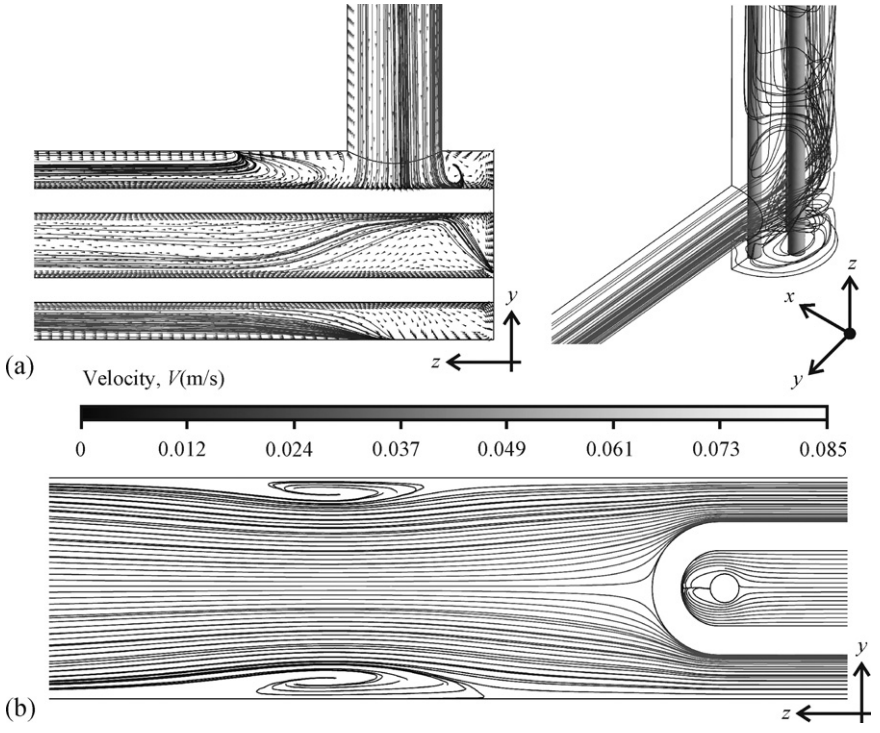

Fig. 14. Stream lines at the heater section for a Q_{heater} =1000 W (a) at the heater inlet and (b) region after the heater.

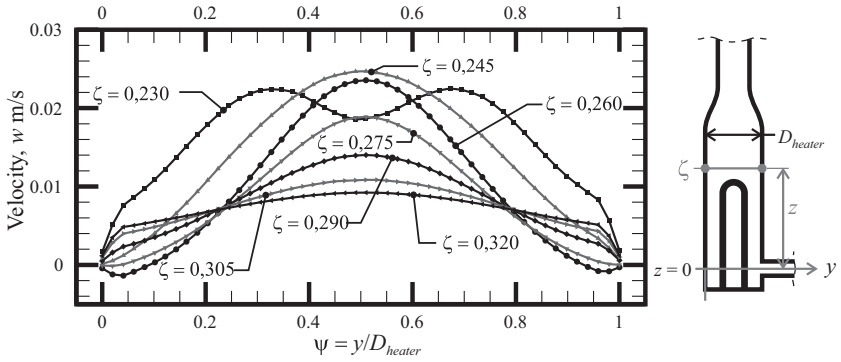

Fig. 15. Velocity profile after the heater region ($0.230 \leqslant \zeta \leqslant 0.320$) for a Q_{heater} =1000 W.

The velocity profiles presented in Fig. 13 are consistent with the natural convection phenomenon (Betts and Bokhari, 2000; Ampofo and Karayiannis, 2003; Choi et al., 2004) in which the maximum speed is obtained near the heated surface. Posterior to the heater entrance, with an increment of ζ, viscous and buoyancy effects tend to make the velocity profiles symmetrical.

Fig. 15 shows the velocity profiles after the heater, $0.230 \leqslant \zeta \leqslant 0.320$. The fluid layers are observed to be gradually mixed and the velocity profiles are constantly modified. For the condition in which ($\zeta = 0.320$), the velocity profile is similar to the turbulent forced convection velocity profiles found in ducts, which suggests that the system behavior may be changing from free convection to a combination of forced plus free convection.

Fig. 16 shows the central velocity profiles $\vec{w}$ (velocity vectors in the z direction obtained in the center of the tube) and the central buoyancy force z (Eq. (12)) as a function of $\log(\zeta)$ for a $Q_{heater} = 1000\,W$. Central profile is understood as the variable or property taken on the tube centerline ($r = 0$).

The velocity magnitude is also relatively small, so the velocity profiles become fully developed in short distances, minimizing the errors due to the use of one-dimensional models. As suggested by several authors (Mertol et al., 1982; Bernier and Baliga, 1992; Su and Chen, 1995; Misale et al., 1999; Basran and Kücüka, 2003), the combined approach, i.e. one-dimensional treatment in the duct posterior to the heaters and two-dimensional treatment in the heater region, may be a viable alternative for reducing the computational domain.

The velocity magnitude is also relatively small, so the velocity profiles are fully developed in short distances, minimizing the errors due to the use of one-dimensional models. As suggested by several authors (Mertol et al., 1982; Bernier and Baliga, 1992; Su and Chen, 1995; Misale et al., 1999; Basran and Kücüka, 2003), the combined approach, i.e. one-dimensional treatment in the duct posterior to the heaters and two-dimensional treatment in the heater region, may be a viable alternative for reducing the computational domain.

There is a geometric contraction from 76.2 mm at $\zeta = 0.338$ to 38 mm at $\zeta = 0.369$ immediately after the heater.

Fig. 17 shows the central velocity and temperature profiles in the heat exchanger region for a $Q_{heater} = 1000\,W$.

In the heat exchanger region, there is a velocity fluctuation due to the contraction and expansion of the flow (Fig. 17), which changes the heat transfer. Classical one-dimensional models for relatively complex geometries (as the case of this exchanger) fail to capture such an effect.

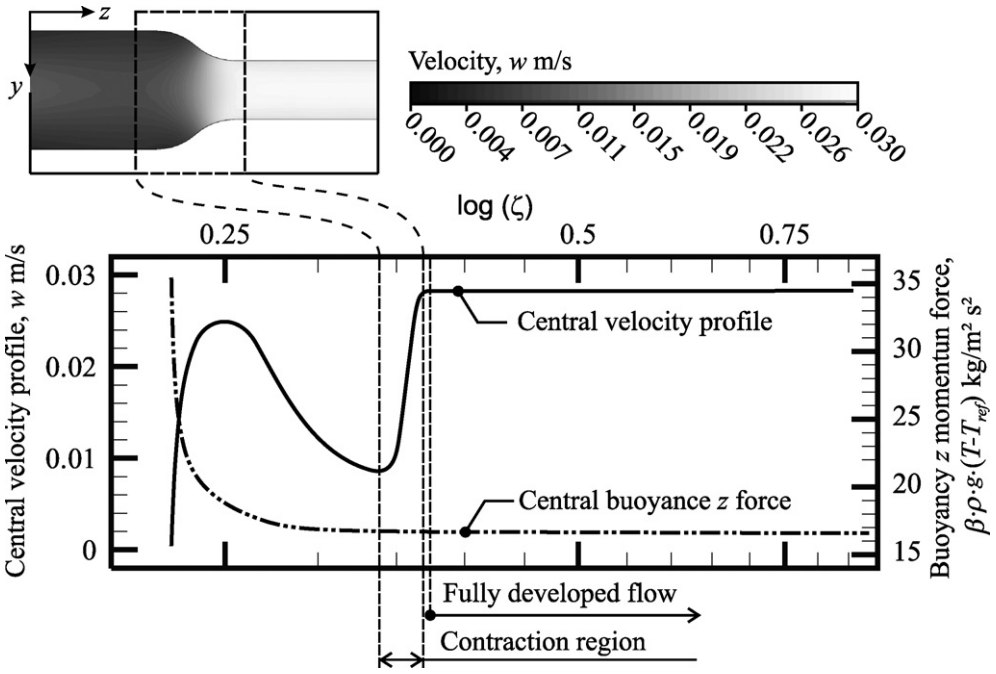

Fig. 16. Central velocity profile and central buoyancy z force versus $\log(\zeta)$ for a Q_{heater} =1000 W.

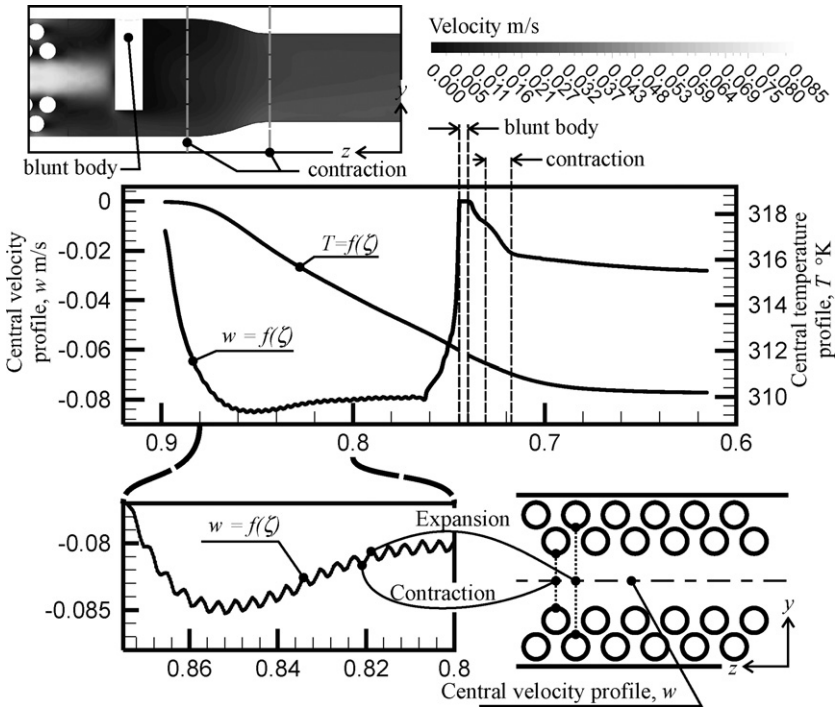

Fig. 17. Central velocity profile and central temperature profile for a Q_{heater} =1000 W in heat exchanger region.

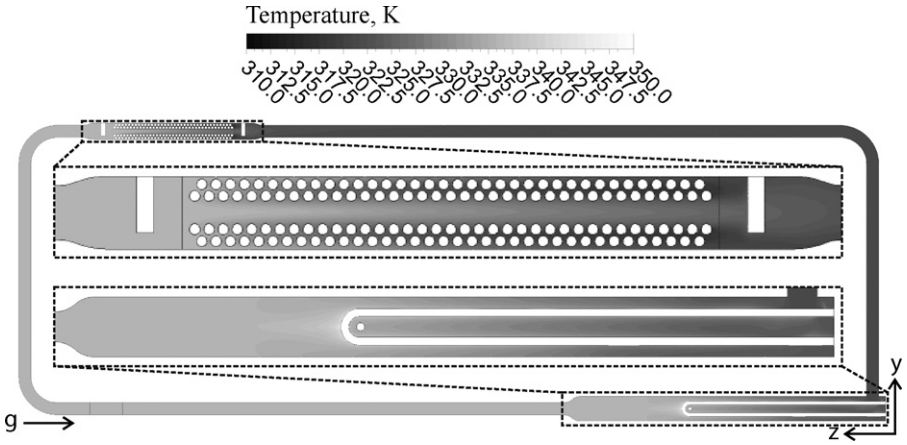

Fig. 18. Velocity contour for a Q_{heater} =2500 W.

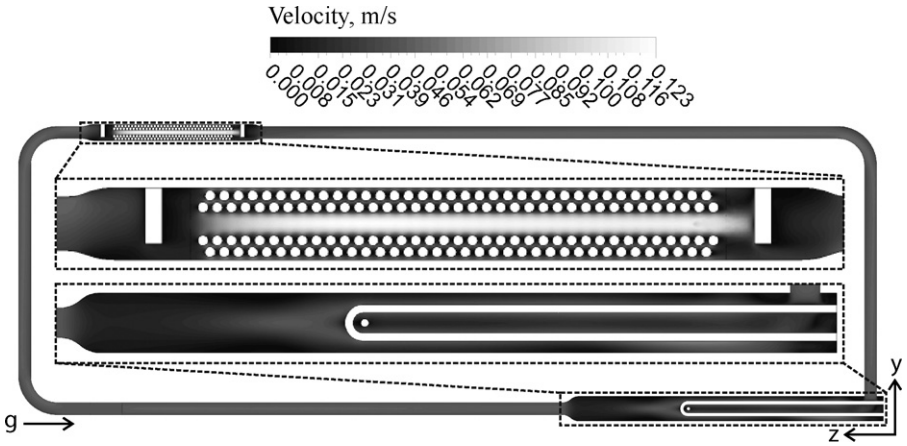

Fig. 19. Temperature contour for a Q_{heater} =2500 W.

Figs. 18 and 19 present the velocity and temperature contours, respectively, for a power of 2500 W at heater 1.

5. Conclusions

The natural circulation loop in steady state and single-phase condition was simulated in 3-D resulting in a good agreement between the numerical results and the measurements.

The simplified geometry and boundary conditions imposed on the heat exchanger overestimated the overall heat transfer rate. This fact is justified by the geometric simplifications assumption.

The three-dimensional effects, such as the formation of vortex structures and swirl effects, were captured at the entrance and after the heater (Figs. 14a and b).

Aspects to create a robust model as the mesh quality and dependency were verified in this development. Simulations showed that the numerical model, presented in this paper, led to consistent results. It was able to capture the velocity fluctuation at the heat exchanger due to cross sectional area variations, which is very positive, since the classical one-dimensional models for relatively complex geometries, as the case of this exchanger, fail to capture this effect.

However, since the three-dimensional simulation is very costly in terms of computational time, the coupling between the one-dimensional and three-dimensional models for regions where there are no complex geometries (e.g. pipelines) could be a viable alternative for reducing the number of elements in three-dimensional simulations as well as for studying the global dynamics of the flow.

Acknowledgments

The authors would like to acknowledge the following organization:

Conselho Nacional de Desenvolvimento Científico e Tecnológico (CNPQ).

References

Ambrosini, W., Forgione, N., Ferreri, J., Bucci, M., 2004. The effect of wall friction in single-phase natural circulation stability at the transition between laminar and turbulent flow. Annals of Nuclear Energy 31 (16), 1833–1865.

Ampofo, F., Karayiannis, T., 2003. Experimental benchmark data for turbulent natural convection in an air filled square cavity. International Journal of Heat and Mass Transfer 46 (19), 3551–3572.

Anderson, J., Wendt, J., 1995. Computational Fluid Dynamics. McGraw-Hill.

ANSYS, C., 2009. 12.0 User's Manual, ANSYS.

Basran, T., Kücüka, S., 2003. Flow through a rectangular thermosyphon at specified wall temperatures. International Communications in Heat and Mass Transfer 30 (7), 1027–1039.

Bernier, M., Baliga, B., 1992. A 1-D/2-D model and experimental results for a closed-loop thermosyphon with vertical heat transfer sections. International Journal of Heat and Mass Transfer 35 (11), 2969–2982.

Betts, P., Bokhari, I., 2000. Experiments on turbulent natural convection in an enclosed tall cavity. International Journal of Heat and Fluid Flow 21 (6), 675–683.

Bevington, P., Robinson, D., 1969. Data Reduction and Error Analysis for the Physical Sciences, vol. 336. McGraw-Hill, New York.

Carelli, M., Conway, L., Oriani, L., Petrovi, B., Lombardi, C., Ricotti, M., Barroso, A., Collado, J., Cinotti, L., Todreas, N., et al., 2004. The design and safety features of the IRIS reactor. Nuclear Engineering and Design 230 (1–3), 151–167.

Choi, S., Kim, E., Wi, M., Kim, S., 2004. Computation of a turbulent natural convection in a rectangular cavity with the low-Reynolds-number differential stress and flux model. Journal of Mechanical Science and Technology 18 (10), 1782–1798.

Desrayaud, G., Fichera, A., Marcoux, M., 2006. Numerical investigation of natural circulation in a 2d-annular closed-loop thermosyphon. International Journal of Heat and Fluid Flow 27 (1), 154–166.

Greif, R., 1988. Natural circulation loops. Journal of Heat Transfer 110, 1243.

Huang, B., Zelaya, R., 1988. Heat transfer behavior of a rectangular thermosyphon loop. Journal of Heat Transfer 110, 487.

IAEA-TECDOC, 2005. Natural circulation water cooled nuclar power plants: phenomena, models, and methodology for system reliability assessments. International Atomic Energy Agency 1474.

Incropera, F., De Witt, D., 1985. Fundamentals of Heat and Mass Transfer. John Wiley and Sons Inc., New York, NY.

Ingersoll, D., 2009. Deliberately small reactors and the second nuclear era. Progress in Nuclear Energy 51 (4–5), 589–603.

Jiang, Y., Shoji, M., Naruse, M., 2002. Boundary condition effects on the flow stability in a toroidal thermosyphon. International Journal of Heat and Fluid Flow 23 (1), 81–91.

Launder, B., Spalding, D., 1974. The numerical computation of turbulent flows. Computer Methods in Applied Mechanics and Engineering 3 (2), 269–289.

Lavine, A., Greif, R., Humphrey, J., 1987. A three-dimensional analysis of natural convection in a toroidal loop-the effect of Grashof number. International Journal of Heat and Mass Transfer 30 (2), 251–262.

Maliska, C., 1994. Transferência de calor e mecânica dos fluidos computacional: fundamentos e coordenadas generalizadas. Livros Técnicos e Cientí ficos.

Mertol, A., Greif, R., Zvirin, Y., 1982. Two-dimensional study of heat transfer and fluid flow in a natural convection loop. Journal of Heat Transfer 104, 508.

Misale, M., RUFFINO, P., Frogheri, M., 1999. The influence of the wall thermal capacity and axial conduction over a single-phase natural circulation loop: 2-D numerical study. In: EUROTHERM Seminar, pp. 177–186.

Pilkhwal, D., Ambrosini, W., Forgione, N., Vijayan, P., Saha, D., Ferreri, J., 2007. Analysis of the unstable behaviour of a single-phase natural circulation loop with one-dimensional and computational fluid-dynamic models. Annals of Nuclear Energy 34 (5), 339–355.

Stern, F., Wilson, R., Coleman, H., Paterson, E., 2001. Comprehensive approach to verification and validation of CFD simulations-Part 1. Methodology and procedures. Transactions-American Society of Mechanical Engineers Journal of Fluids Engineering 123 (4), 793–802.

Su, Y., Chen, Z., 1995. 2-D numerical study on a rectangular thermosyphon with vertical or horizontal heat transfer sections. International Journal of Heat and Mass Transfer 38 (17), 3313–3317.

Teertstra, P., Yovanovich, M., Culham, J., 2006. Modeling of natural convection in electronic enclosures. Journal of Electronic Packaging 128, 157.

Vijayan, P., 2002. Experimental observations on the general trends of the steady state and stability behaviour of single-phase natural circulation loops. Nuclear Engineering and Design 215 (1–2), 139–152.

Wilson, R., Stern, F., Coleman, H., Paterson, E., 2001. Comprehensive approach to verification and validation of CFD simulations. 2. Application for RANS simulation of a cargo/container ship. Journal of Fluids Engineering 123 (4), 803–810.

Zvirin, Y., 1982. A review of natural circulation loops in pressurized water reactors and other systems. Nuclear Engineering and Design 67 (2), 203–225.